Heliyon 10 (2024) e38640

Contents lists available at ScienceDirect

Heliyon

journal homepage: www.cell.com/heliyon

Research article

Leveraging MRI radiomics signature for predicting the diagnosis of CXCL9 in breast cancer

Liping Yan [a,b], Yuexia Chen [c], Jianxin He [d,*]

[a] Department of Breast Surgery, Maternal and Child Health Hospital of Jiangxi Province, Nanchang, China
[b] Department of Surgery, the First Affiliated Hospital of Guangxi Medical University, China
[c] Department of Pathology, The Third Hospital of Nanchang, Nanchang, China
[d] Department of Ultrasound Medicine, The First Affiliated Hospital of Nanchang University, China

ARTICLE INFO

Keywords:
Breast cancer
CXCL9
MRI
Radiomic
Non-invasive diagnosis

ABSTRACT

Objective: A non-invasive predictive model was developed using radiomic features to forecast CXCL9 expression level in breast cancer patients.
Methods: CXCL9 expression data and MRI images of breast cancer patients were obtained from The Cancer Genome Atlas (TCGA) and The Cancer Imaging Archive (TCIA) databases, respectively. Local tissue samples from 20 breast cancer patients were collected to measure CXCL9 expression levels. Radiomic features were extracted from MRI images using 3DSlicer, and the minimum Redundancy Maximum Relevance and Recursive Feature Elimination (mRMR_RFE) method was employed to select the most pertinent radiomic features associated with CXCL9 expression levels. Support vector machine (SVM) and Logistic Regression (LR) models were utilized to construct the predictive model, and the area under the receiver operating characteristic curve (AUC) was calculated for performance evaluation.
Results: CXCL9 was found to be upregulated in breast cancer patients and linked to breast cancer prognosis. Nine radiomic features were ultimately selected using the mRMR_RFE method, and SVM and LR models were trained and validated. The SVM model achieved AUC values of 0.748 and 0.711 in the training and validation sets, respectively. The LR model obtained AUC values of 0.771 and 0.724 in the training and validation sets, respectively.
Conclusion: The utilization of MRI radiomic features for predicting CXCL9 expression level provides a novel non-invasive approach for breast cancer Prognostic research.

1. Introduction

Breast cancer is among the most prevalent malignancies in women, with over two million individuals diagnosed with the disease each year globally [1–3]. The current gold standard for diagnosis of breast cancer via tissue biopsy [4]. The diagnosis of breast cancer lacks traditional biomarkers. Despite advancements in the early diagnosis and management that have enhanced prognosis the complexities of early detection and the invasive nature of certain diagnostic approaches often cause significant distress for those affected.

MRI is a widely used diagnostic modality for breast cancer, recognized for its high resolution and operational simplicity [5,6]. Previous radiomics studies have demonstrated that radiomic models can effectively predict breast cancer prognosis, identify

* Corresponding author.
E-mail address: 286503805@qq.com (J. He).

https://doi.org/10.1016/j.heliyon.2024.e38640
Received 24 February 2024; Received in revised form 26 September 2024; Accepted 26 September 2024
Available online 28 September 2024

pathological subtypes, and assess treatment responses [7–9]. Furthermore, radiomics models can predict the lymph node status of breast cancer, serving as an important basis for supporting surgical decision-making [10,11]. Imaging studies utilizing MRI semantic features have demonstrated that these features can predict TIL levels in breast cancer, suggesting that MRI data can foresee the microscopic molecular phenotype of tumors [12]. Radiomics involves extracting and analyzing features from various imaging modalities, such as gray-level histogram characteristics and morphological features, which are not visible to the naked eye. This enables for quantification of tumor heterogeneity [13,14].It has been extensively utilized in various fields including disease diagnosis, assessment of biological behavior, and prognostic evaluation and demonstrating significant potential noninvasive preoperative assessment of tumor molecular subtyping [15,16].

The assessment of the tumor immune microenvironment plays a crucial role in predicting the prognosis of breast cancer [17]. CXCL9, a pivotal molecule involved in immune regulation and inflammation processes and belonging to the chemokine superfamily, stimulated JAK/STAT activity, thereby modulating the tumor microenvironment [18]. Previous studies have indicated that high expression levels of CXCL9 are linked to a poor prognosis in breast cancer [19,20]. In a randomized trial involving 557 patients tested for CXCL9 mRNA, high CXCL9 expression was found to be a negative prognostic indicator for overall survival (OS), with a hazard ratio (HR) of 1.73 and a P-value of 0.021 [21]. Breast cancer cells stimulate the growth of lung metastases by triggering the production of CXCL9 and CXCL10 in lung fibroblasts via NF-κB signaling [22]. Currently, the assessment of CXCL9 molecular expression levels in breast cancer primarily relies on invasive immunohistochemical (IHC) analysis of biopsy specimens. However, these methods are costly, time-consuming, and invasive. A large number of studies have highlighted the inter-laboratory variation in diagnostic IHC tests and the inability to quantitatively and objectively assess immunostaining sensitivity [23].Therefore, there is a demand for more efficient approaches to assess the expression levels of CXCL9 in breast cancer.

Previous radiomics studies have demonstrated that radiomics models can effectively predict breast cancer prognosis, pathological subtypes, and treatment responses [7–9]. Additionally, these models have demonstrated the ability to predict lymph node status in breast cancer, providing crucial support for surgical decision-making [10,11]. Imaging studies using MRI semantic features have also revealed that these features can predict tumor-infiltrating lymphocyte (TIL) levels in breast cancer, indicating that MRI has the potential to predict the tumor's microscopic molecular phenotype [12]. However, despite CXCL9 being a significant molecular marker in breast cancer, no radiomics model currently exists to predict CXCL9 expression. Our study introduces a novel, non-invasive prediction model for CXCL9 expression in breast cancer, distinguishing it from previous models. Thus, our investigation endeavors to develop a sophisticated radiomic model by leveraging comprehensive data from the esteemed Cancer Genome Atlas (TCGA) and the Cancer Imaging Archive (TCIA) to accurately predict CXCL9 expression in breast cancer (BC) patients. Additionally, we seek to demonstrate that predicting CXCL9 expression levels provides a novel non-invasive radiomic model approach for breast cancer diagnostic research.

2. Methods

2.1. Sources of data and images

Data and images for this study are obtained from The Cancer Genome Atlas (TCGA) and The Cancer Imaging Archive (TCIA), including dynamic contrast-enhanced magnetic resonance imaging (DCE-MRI) images, clinical information, and gene expression data for CXCL9. The RNA-seq data from TCGA and GTEx in TPM format were uniformly using the Toil workflow [24] by log2 transformation. Differential expression analysis was performed to identify gene expression differences between samples. Using the R package "survminer" with a Cutoff value of 3.963, genes were categorized into high and low expression groups. Upload the gene expression matrix of breast cancer samples to the CIBERSORTx database (https://cibersortx.stanford.edu/) to evaluate immune cell infiltration for each sample. Utilize the R package "limma" to analyze the differences in immune cell infiltration between high and low expression of CXCL9. Using GSVA, pathway enrichment scores for KEGG and Hallmark gene sets were calculated in each sample, and differential analysis on high and low CXCL9 groups was conducted using the R package "limma". An exploratory subgroup analysis was performed using univariate COX regression to evaluate the impact of CXCL9 (high expression group vs. low expression group) on patient prognosis across various covariate subgroups. The likelihood ratio test was employed to analyze the interaction between CXCL9 expression and other covariates.

2.2. Immunohistochemistry

Breast cancer tissue and adjacent tissue specimens were collected from patients at the First Affiliated Hospital of Guangxi Medical University. This study was reviewed and approved by the Medical Ethics Committee of the First Affiliated Hospital of Guangxi Medical University and informed consent was obtained from the patients (NO.2023-S510-01). The specimens were processed for immunohistochemistry by fixing, embedding, and preparing 4-micron-thick slices. The slices were subjected to antigen retrieval using high-pressure steam treatment and then blocked with 10 % bovine serum. Rabbit anti-human CXCL9(Bioss bs-2551R) antibody was added to the slices and incubated overnight. The next day, HRP-labeled secondary antibodies (Servicebio GB23303) were applied, followed by color development using DAB. The stained slices were analyzed quantitatively for CXCL9 expression using Image Pro Plus.

2.3. Radiomics feature extraction and model establishment

DICOM images of 101 patients were obtained from the TCIA image database and segmented using 3D Slicer software (version 4.10.2). The tumor region with the most significant enhancement on the MRI was manually delineated by an experienced radiologist to

obtain the complete tumor area. Z-score normalization of images reduces noise and standardizes intensity, minimizing variations in signal strength from different machines. In addition, to assess the stability of radiomics features, another attending physician randomly selected 20 samples for delineation and identified the radiomics features with an Intraclass Correlation Coefficient (ICC) value of $\geq$0.75.

The data was randomly divided into training and validation sets in a 6:4 ratio. Radiomics features from both the training and validation sets were standardized, and the differences in clinical variables between the two groups were analyzed. The mRMR_RFE method was used to select the radiomics features most correlated with CXCL9 expression levels. Prediction models were then built using support vector machine (SVM) [25,26]and logistic regression (LR) (Radiomics Formula = Feature × Corresponding Coefficient (Estimate) + Intercept Value (Estimate)) [27]. The calibration and clinical benefit of the radiomics prediction model were assessed by plotting calibration curves and conducting decision curve analysis (DCA) [28,29]. The probability that the radiomics model uses to predict gene expression levels is defined as the Rad_score. Spearman analysis was used to assess the correlation between Rad_score and immune-related gene [30] expression levels.

2.4. Statistical analysis

The numerical data were presented as mean ± standard deviation (mean ± SD), while the categorical data were represented using relative frequency and percentage. Chi-square test was used to compare the baseline characteristics of categorical variables. Spearman correlation analysis was conducted to assess the correlation between rad_score and other covariates or genes. Kaplan-Meier method was employed to plot survival curves, and log-rank test was used for between-group comparisons. Cox proportional hazards regression analysis was performed to evaluate the impact of various covariates on patient prognosis in different subgroups. Statistical significance was defined as a two-sided p-value <0.05. All statistical analyses were conducted using R software (version 4.1.1).

3. Results

3.1. Identification of CXCL9 as a differentially expressed gene

3.1.1. Patient characteristics

A total of 928 patients were included in the TCGA-BC database, with 464 patients in the CXCL9 high-expression group and 464 patients in the low-expression group, using a cutoff value of 3.963 for expression levels (Fig. 1). No significant differences between the high and low expression groups, except for age (P = 0.015). Baseline characteristics of patients in the TCGA-BC dataset are summarized in Table 1.

3.1.2. Difference and enrichment analysis of CXCL9

The results showed that the CXCL9 gene expression level was significantly higher in tumor tissues compared to normal tissues, with a median difference of 2.648 (2.415–2.892) (P < 0.001) (Fig. 2A). This finding was also validated in immunohistochemistry experiments using clinical samples, where the difference was statistically significant (P < 0.001) (Fig. 2B–D). Enrichment analysis of

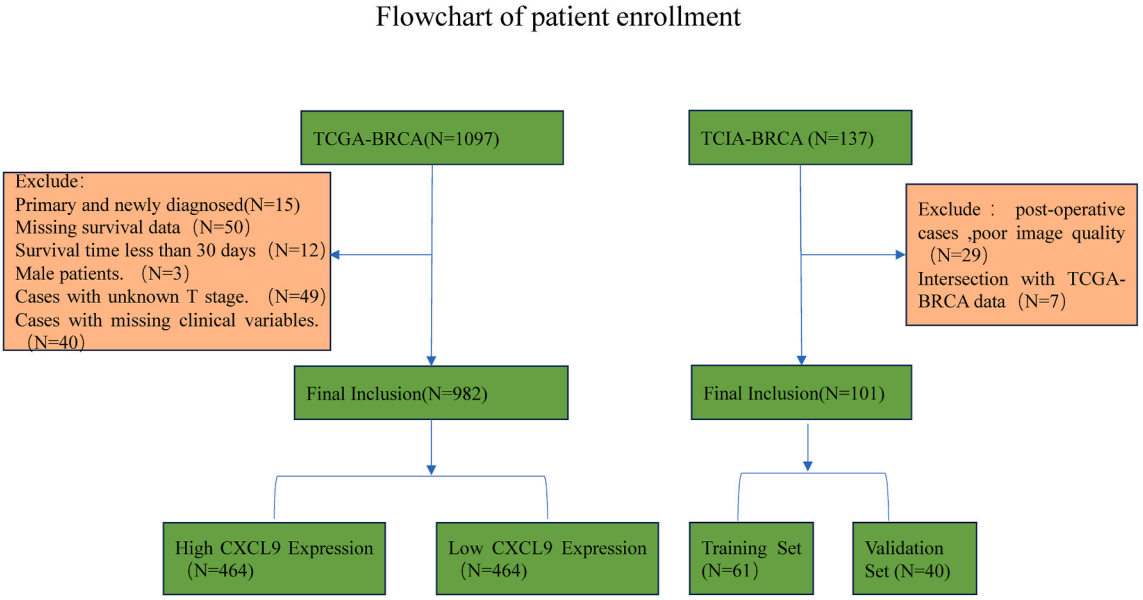

Fig. 1. Flow chart of patient enrolment.

Table 1
Baseline characteristics of CXCL9.

Variables	Total (n = 928)	Low (n = 464)	High (n = 464)	p
Age, n (%)				0.015
~59	506 (55)	234 (50)	272 (59)	
60~	422 (45)	230 (50)	192 (41)	
T_stage, n (%)				0.011
T1	250 (27)	135 (29)	115 (25)	
T2	528 (57)	242 (52)	286 (62)	
T3/T4	150 (16)	87 (19)	63 (14)	
N_stage, n (%)				0.323
N0	430 (46)	223 (48)	207 (45)	
N1/N2/N3/NX	498 (54)	241 (52)	257 (55)	
M_stage, n (%)				0.22
M0	771 (83)	378 (81)	393 (85)	
M1/MX	157 (17)	86 (19)	71 (15)	
ER_status, n (%)				<0.001
Negative	210 (23)	65 (14)	145 (31)	
Positive	718 (77)	399 (86)	319 (69)	
PR_status, n (%)				<0.001
Negative	298 (32)	116 (25)	182 (39)	
Positive	630 (68)	348 (75)	282 (61)	
HER2_status, n (%)				<0.001
Negative	493 (53)	241 (52)	252 (54)	
Positive	140 (15)	52 (11)	88 (19)	
Unknown	295 (32)	171 (37)	124 (27)	
Histological_type, n (%)				0.026
Infiltrating Lobular Carcinoma	185 (20)	91 (20)	94 (20)	
Infiltrating Ductal Carcinoma	655 (71)	317 (68)	338 (73)	
Other	88 (9)	56 (12)	32 (7)	
Margin_status, n (%)				0.853
Negative	778 (84)	386 (83)	392 (84)	
Positive/Close	99 (11)	52 (11)	47 (10)	
Unknown	51 (5)	26 (6)	25 (5)	
Radiotherapy, n (%)				0.1
NO	442 (48)	234 (50)	208 (45)	
YES	486 (52)	230 (50)	256 (55)	
Chemotherapy, n (%)				<0.001
NO	406 (44)	236 (51)	170 (37)	
YES	522 (56)	228 (49)	294 (63)	

CXCL9's differentially expressed genes (DEGs) in breast cancer revealed significant enrichment in signaling pathways such as apoptosis and G2M checkpoint in the low-expression group, based on Hallmark gene set (Fig. 2E). Similarly, in the KEGG gene set, the low-expression group of CXCL9 was significantly enriched in B-cell receptor signaling pathway and apoptosis signaling pathway (Fig. 2F).

3.1.3. Prognostic analysis of CXCL9

The median survival time was 130.87 months in the low-expression group of CXCL9, and 148.53 months in the high-expression group. Kaplan-Meier curves showed that high expression of CXCL9 was associated with improved overall survival (OS) with statistical significance (P = 0.024) (Fig. 3A).

In subgroup analysis, it was observed that high CXCL9 expression, age under 59, absence of nodal (N0) and distant metastasis (M0), and receiving chemotherapy were all protective factors for overall survival (OS) (Fig. 3B–H). The interaction test displayed a p-value of 0.85, indicating no statistical significance. This suggests that there's no significant interaction between CXCL9 and different ER and PR statuses in the subgroups. Essentially, the impact of CXCL9 on OS appears to be similar across the subgroups categorized by ER and PR status (Fig. 3I–J).

3.2. Construction and evaluation of the radiomic model

3.2.1. Consistency evaluation, feature selection

The dataset was randomly split into training and validation sets in a ratio of 6:4, with 61 and 40 cases, respectively. The P-values for age variable differences between the two groups were all greater than 0.05, indicating that the baseline characteristics of the patients in the training and validation sets were comparable. The median ICC value of the radiomic features was 0.977, and the consistency of the two datasets was verified by calculating the consistency ICC coefficient. We identified 103 radiomics features with ICC values greater than 0.75(S Table 1). Subsequently, we employed mRMR and RFE to select 9 representative features. These features were used to train SVM and LR model to predict gene expression levels (Fig. 4).

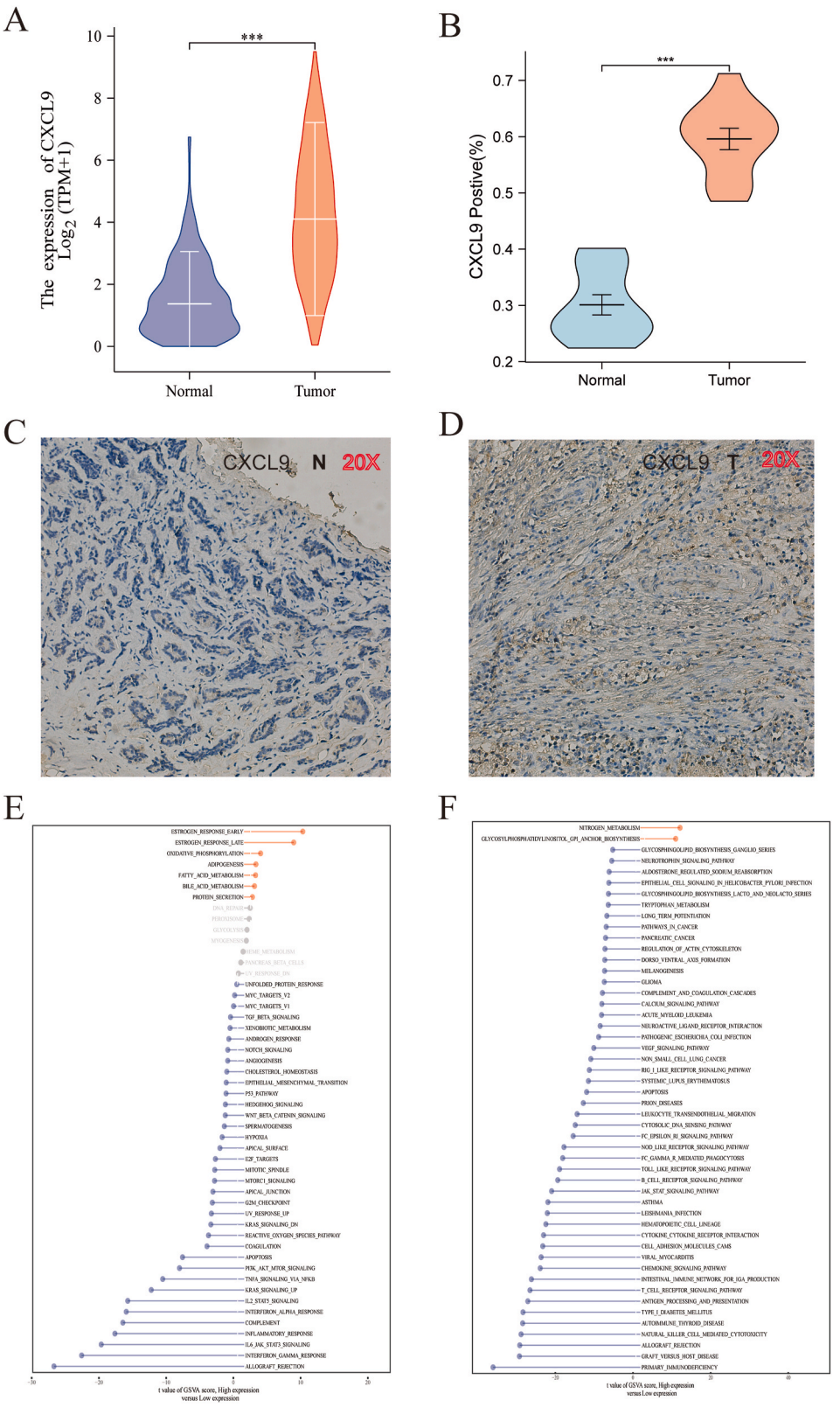

(caption on next page)

Fig. 2. Difference and enrichment analysis of CXCL9:A: The expression of CXCL9 between normal and tumor tissues in the TCGA-BC dataset: The expression of CXCL9 between normal and tumor tissues in our dataset; C–D: The immunohistochemistry of normal and tumor tissues in breast cancer; E–F: Enrichment analysis of CXCL9.

3.2.2. Establishment and evaluation of SVM model

The ROC curves showed that the AUC values of the SVM model in the training set were 0.748, while in the validation set, they were 0.711(Fig. 5A and B). The calibration curves and the Hosmer-Lem show goodness-of-fit test demonstrated good consistency between the predicted probabilities of high gene expression by the radiomics model and the actual values, with p-values of 0.289 for the training set and 0.103 for the validation set (Fig. 5C and D). The decision curve analysis (DCA) revealed that the model had high clinical utility (Fig. 5E and F).

The radiomics model outputted the probability of gene expression levels as Rad_score in the training set, Rad_score values significantly differed between the high and low gene expression groups ($p < 0.05$), with higher Rad_score values in the high expression group. Similar results were observedin the validation set ($p < 0.001$) (Fig. 5G and H), indicating that the SVM model had good predictive performance.

3.2.3. Establishment and evaluation of LR model

After using mRMR and RFE methods to select features, 9 representative imaging features were chosen and fitted using a logistic regression (LR)algorithm to establish a binary classification model for predicting gene expression. The ROC curve showed that the model had an AUC value of 0.771 for the training set and 0.724 for the validation set (Fig. 6A and B). The calibration curve and Hosmer-Lem show goodness-of-fit test showed good consistency between the predicted probabilities and true values for gene expression ($P > 0.05$), with $P = 0.951$ for the training set and $P = 0.116$ for the validation set (Fig. 6C and D). DCA analysis showed that the model had high clinical usability (Fig. 6E and F). The Rad_score in the training set was significantly different between the high and low gene expression groups ($p < 0.001$), and in the validation set, it was significantly different with a p-value of <0.05(Fig. 6G and H). This suggests that the LR model also has a good predictive performance.

3.3. Correlation between rad-score and immune-related genes

Delong's test was used to compare the AUC values of SVM and LR models, revealing no statistically significant differences in either the training or validation sets ($p = 0.732$ and $p = 0.646$, respectively), indicating excellent model fitting. Furthermore, there were no statistically significant differences in AUC values between the training and validation sets for both models ($p = 0.374$ and 0.816), suggesting robust predictive capabilities. However, the LR model performed slightly better than the SVM model in terms of AUC and ACC, so the LR model was used to perform Spearman correlation analysis with immune-related genes. The results showed a positive correlation between Rad_score and cxcl9, and PDCD1 genes, with correlation coefficients of $r = 0.4$ $p < 0.01$, and $r = 0.49$, $p < 0.001$, respectively. There was also a positive correlation between cxcl9 and PDCD1 genes, with a correlation coefficient of 0.88, $p < 0.001$. This indicates a significant correlation between Rad_score and the expression levels of CXCL9 and PDCD1(Fig. 7).

4. Discussion

In this study utilizing MRI-based radiomics-molecular analysis, our objective was to elucidate the interrelation between radiomics features extracted from pre-treatment breast cancer MRI images and the expression levels of CXCL9, a chemokine receptor known to facilitate invasion and metastasis [22]. Given the considerable heterogeneity of breast cancer, augmenting prognostic information holds promise for enhancing clinical decision-making. Notably, CXCL9 has been implicated in breast cancer prognosis in prior research [20]. Kaplan-Meier curve analysis revealed a favorable prognosis in patients with high CXCL9 expression, and multivariate analysis confirmed CXCL9 as an independent adverse prognostic factor for overall survival in breast cancer patients. The imaging changes are the macroscopic manifestations of the changes of microscopic components (molecules, cells, etc.), and changes in the CXCL9 molecule may serve as the molecular pathological basis behind the imaging signs or omics. Numerous observational studies have reported that radiomics features have powerful predictive and discriminative for ER, PR and molecular subtypes of breast cancer [31,32]. Animal studies have shown the causal relationship between radiomics features and molecules by intervening molecular expression [33,34]. Recent articles further demonstrate that imaging phenotyping models exhibit similarities across different species [35]. The diagnostic model developed in this study, incorporating radiomics features and CXCL9 expression levels, exhibited a significant association, thus enabling non-invasive prediction of CXCL9 expression levels and fostering individualized clinical decision-making.

MRI diagnosis solely relies on morphological features, which may lack an objective and quantitative approach. In contrast, radiomics, a cutting-edge approach, can extract high-dimensional features from medical images, uncovering hidden information that is not visually apparent, and enabling quantitative analysis for improved diagnosis and treatment planning.

In this study, we extracted DCE-MRI imaging data and employed advanced feature selection methods such as mRMR and RFE to identify highly correlated radiomic features between the CXCL9 high-expression group and CXCL9 low-expression group. Ultimately, 9 representative imaging features were selected. The SVM model achieved AUC values of 0.748 in the training set and 0.711 in the validation set, while the LR model achieved AUC values of 0.771 in the training set and 0.724 in the validation set, demonstrating excellent diagnostic performance. Importantly, the models exhibited consistent performance with comparable AUC values in the training and validation sets, indicating stability. The radiomics score based on the training set showed statistically significant

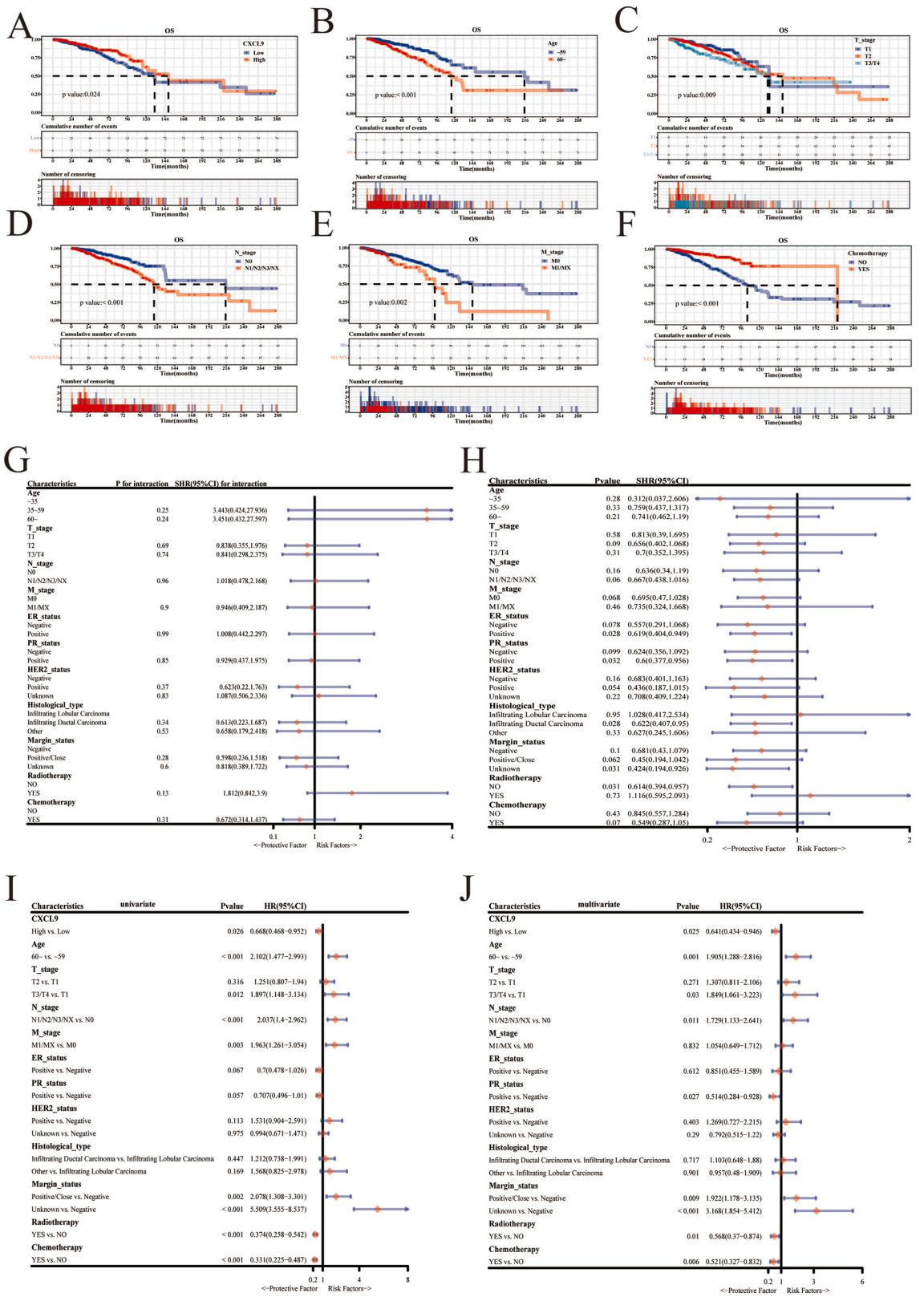

Fig. 3. Prognostic analysis of CXCL9: A–F: the Kaplan-Meier curves of CXCL9 expression, age, T, N, M, and chemotherapy for OS; G–H: Forest plot for univariate and multivariate analysis; I–J: The P value of the characteristics and the interaction test.

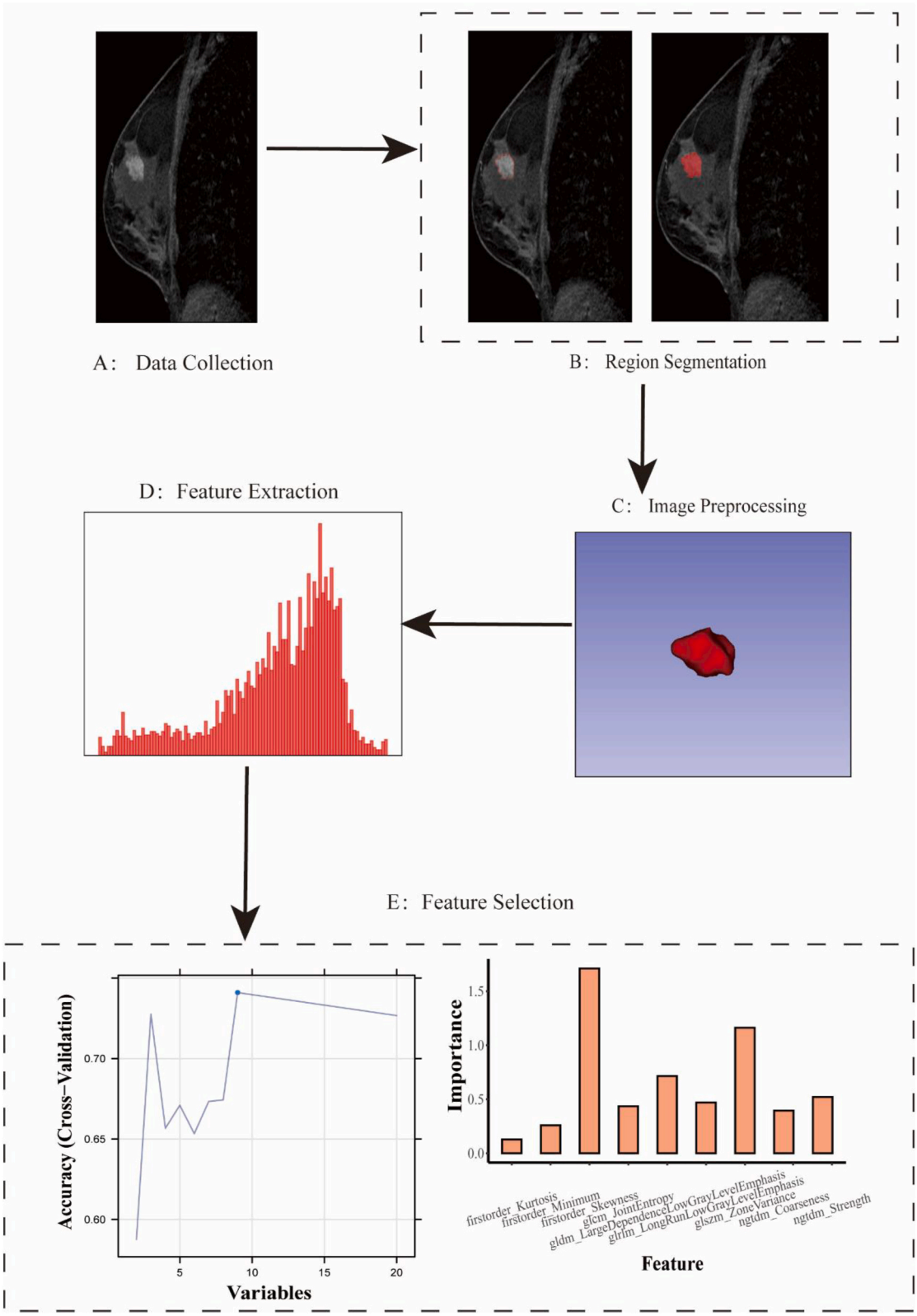

Fig. 4. Workflow of Radiomics: A: Data Collection; B: Image Preprocessing; C: Region Segmentation; D: Feature Extraction; E: Feature selection.

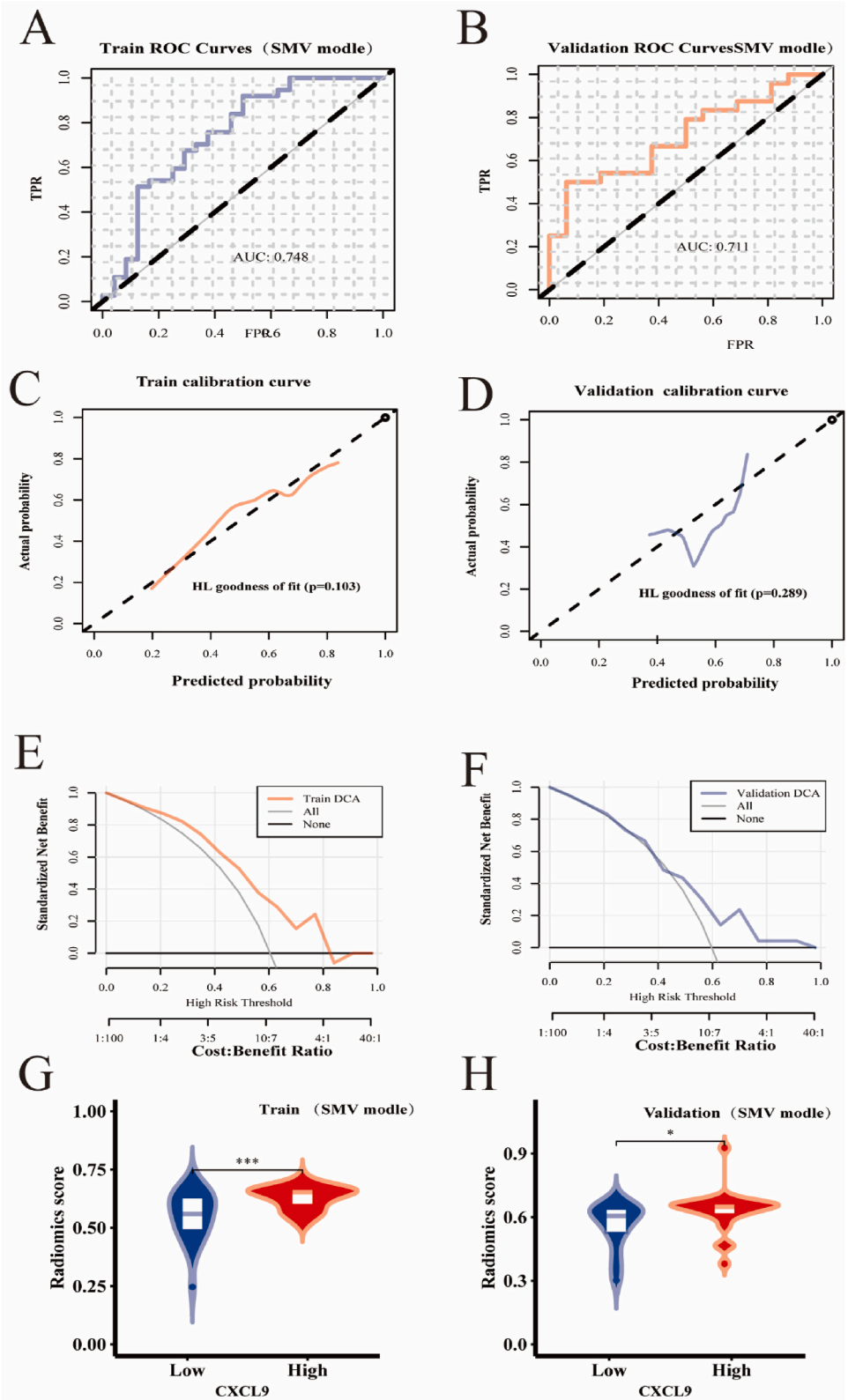

Fig. 5. Establishment and evaluation of SVM model: A, B: The ROC curves of SVM model in the training and validation set; C, D: The calibration curves of SVM model in the training and validation set; E, F: The decision curve analysis of SVM model in the training and validation set; G, H: The Rad_score values between high and low expression level of CXCL9 in the training and validation set.

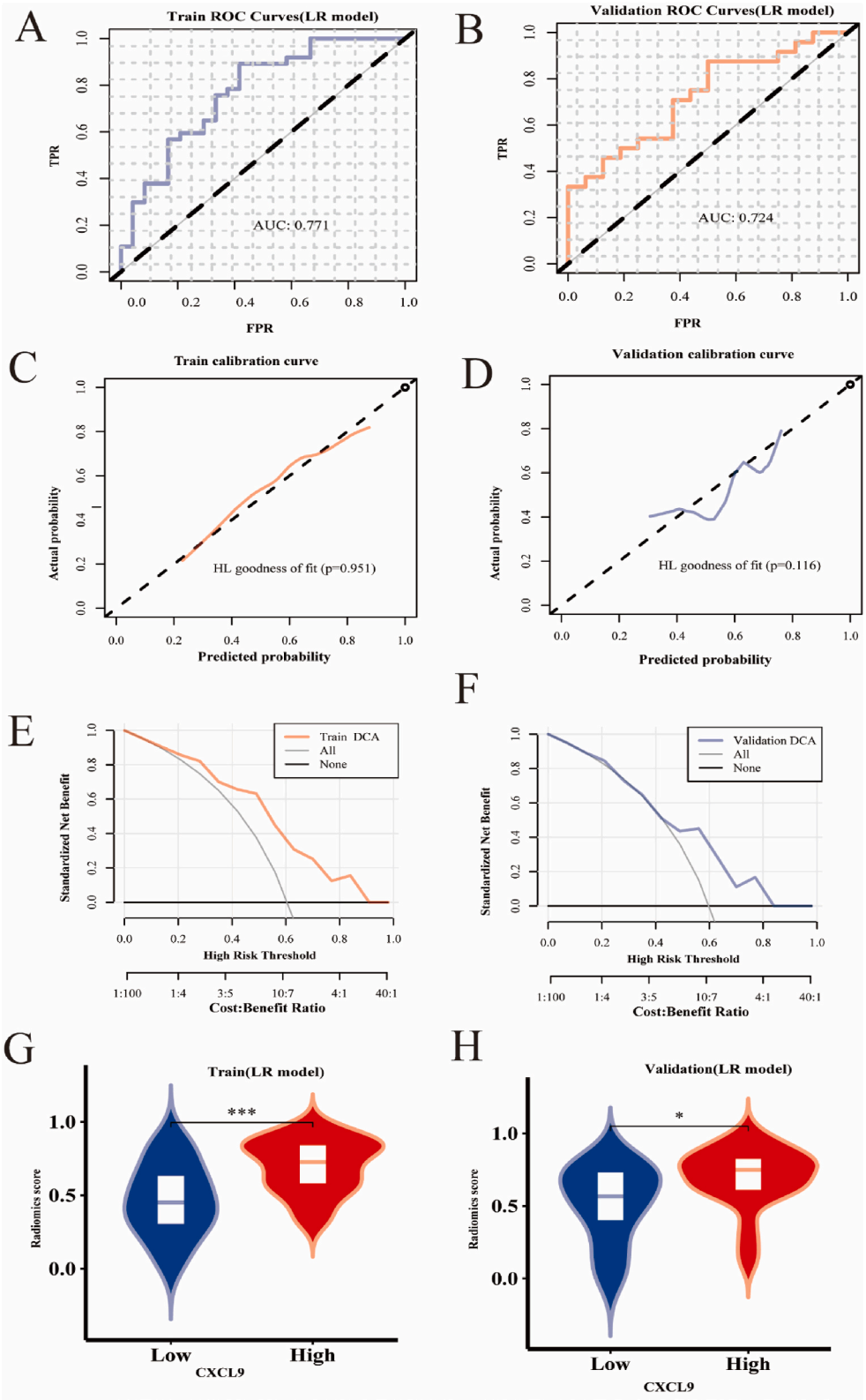

Fig. 6. Establishment and evaluation of LR model: A, B: The ROC curves of LR model in the training and validation set; C, D: The calibration curves of LR model in the training and validation set; E, F: The decision curve analysis of LR model in the training and validation set; G, H: The Rad_score values between high and low expression level of CXCL9 in the training and validation set.

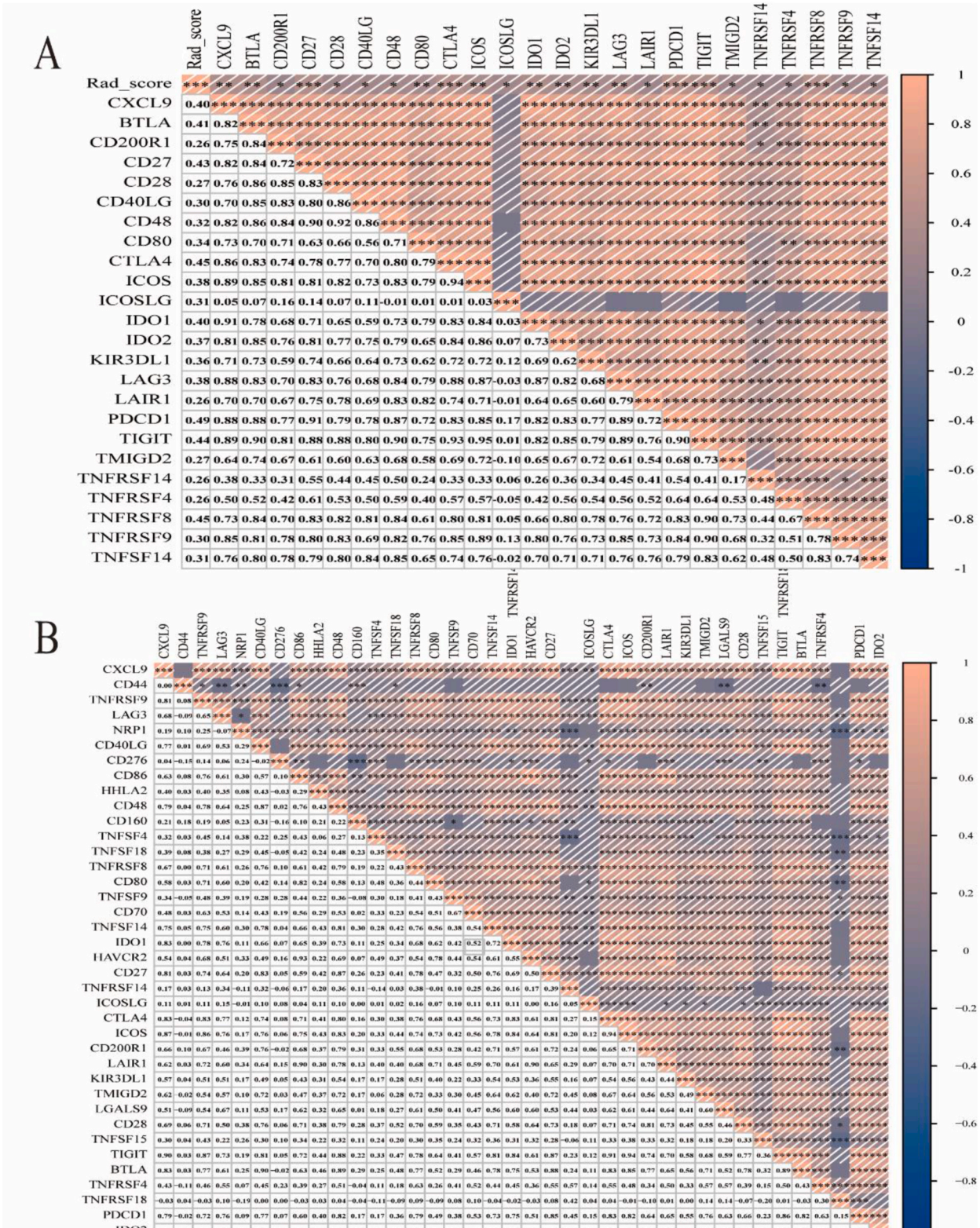

Fig. 7. Correlation between Rad-score and Immune-related genes.

differences between the CXCL9 high-expression and low-expression groups, which were consistent with the results obtained from the validation set. Texture differences among different subregions within the tumor reflected the heterogeneity of imaging. Our predictive model retained 9 radiomic features, including gray-level co-occurrence matrix (GLCM), which has been previously reported to predict improved prognosis in breast cancer distant metastasis [36].

The Rad_score positively correlateswith the expression levels of CXCL9 and PDCD1 genes, with correlation coefficients of $r = 0.4$ ($p < 0.01$) and $r = 0.49$ ($p < 0.001$), respectively. Additionally, CXCL9 exhibits significant correlations with immune cell infiltration and other immune-related biomarkers, including CTLA4, GZMB, LAG3, PDCD1, and HAVCR2. Previous research in breast cancer has identified a positive correlation between CXCL9 and PD-1 [19]. Macrophages within the tumor microenvironment (TME) produce high levels of CXCL9, which plays a crucial role in antitumor immunity. The loss of tumor-associated macrophages (TAMs) can diminish the CXCL9 induced by anti-PD-1 and anti-CTLA-4 therapies, thereby reversing the effectiveness of immunotherapy [37].

These findings suggest that the predictive model constructed based on DCE-MRI radiomics features can effectively and non-invasively predict CXCL9 expression, providing valuable insights for clinical treatment decision-making and personalized therapy for breast cancer patients. However, investigations into the correlation between radiomics and CXCL9 expression levels are in their nascent stage, and certain limitations require attention. This study is retrospective in nature, utilizing data from publicly available databases, and the radiomics features are derived from DCE-MRI sequence modality, known for its substantial image heterogeneity. DCE sequence is the most popular sequence in breast cancer radiomics research [38,39]. Previous radiomics studies of breast cancer has found that DCE sequence has better predictive performance than T2 sequence and DWI sequence [40]. Although we standardized the MRI images, the heterogeneity due to imaging devices and parameters may still affect the radiomics features. In different regions, breast cancer patients have heterogeneity in age and disease characteristics [41].This study was only based on TCGA population, and with limited sample size and scope. Therefore, the prediction performance of the radiomics model in other populations and larger sample sizes remains further verification and exploration.

In conclusion, the expression level of CXCL9 significantly affects the overall prognosis of breast cancer patients. Radiomics scores can noninvasively predict the expression level of CXCL9 and are significantly correlated with other immune genes and immune checkpoint molecules.

Data availability statement

The raw data supporting the conclusions of this article will be made available by the authors, without undue reservation.

Ethics statement

The authors are accountable for all aspects of the work in ensuring that questions related to the accuracy or integrity of any part of the work are appropriately investigated and resolved. The study was conducted in accordance with the Declaration of Helsinki (as revised in 2013)

Funding

None.

CRediT authorship contribution statement

Liping Yan: Writing – original draft, Project administration, Methodology, Investigation, Formal analysis, Data curation, Conceptualization. **Yuexia Chen:** Writing – original draft, Software, Project administration, Methodology, Investigation, Formal analysis. **Jianxin He:** Supervision, Methodology, Investigation, Funding acquisition, Formal analysis.

Declaration of competing interest

The authors declare that they have no known competing financial interests or personal relationships that could have appeared to influence the work reported in this paper.

Appendix A. Supplementary data

Supplementary data to this article can be found online at https://doi.org/10.1016/j.heliyon.2024.e38640.

References

[1] A.N. Giaquinto, H. Sung, K.D. Miller, J.L. Kramer, L.A. Newman, A. Minihan, A. Jemal, R.L. Siegel, Breast cancer statistics, 2022, CA Cancer J Clin 72 (2022) 524–541, https://doi.org/10.3322/caac.21754.

[2] C. Xia, X. Dong, H. Li, M. Cao, D. Sun, S. He, F. Yang, X. Yan, S. Zhang, N. Li, W. Chen, Cancer statistics in China and United States, 2022: profiles, trends, and determinants, Chin Med J (Engl). 135 (2022) 584–590, https://doi.org/10.1097/CM9.0000000000002108.

[3] R.L. Siegel, K.D. Miller, H.E. Fuchs, A. Jemal, Cancer statistics, CA Cancer J Clin. 72 (2022) 7–33, https://doi.org/10.3322/caac.21708, 2022.

[4] T.B. Bevers, M. Helvie, E. Bonaccio, K.E. Calhoun, M.B. Daly, W.B. Farrar, J.E. Garber, R. Gray, C.C. Greenberg, R. Greenup, N.M. Hansen, R.E. Harris, A. S. Heerdt, T. Helsten, L. Hodgkiss, T.L. Hoyt, J.G. Huff, L. Jacobs, C.D. Lehman, B. Monsees, B.L. Niell, C.C. Parker, M. Pearlman, L. Philpotts, L.B. Shepardson, M.L. Smith, M. Stein, L. Tumyan, C. Williams, M.A. Bergman, R. Kumar, Breast cancer Screening and diagnosis, version 3.2018, NCCN clinical practice guidelines in oncology, J. Natl. Compr. Cancer Netw. 16 (2018) 1362–1389, https://doi.org/10.6004/jnccn.2018.0083.

[5] D.G. Nishimura, Principles of Magnetic Resonance Imaging, Stanford University, 1996.

[6] Z. Han, X. Wu, S. Roelle, C. Chen, W.P. Schiemann, Z.R. Lu, Targeted gadofullerene for sensitive magnetic resonance imaging and risk-stratification of breast cancer, Nat. Commun. 8 (2017) 692, https://doi.org/10.1038/s41467-017-00741-y.

[7] A. Conti, A. Duggento, I. Indovina, M. Guerrisi, N. Toschi, Radiomics in breast cancer classification and prediction, Semin. Cancer Biol. 72 (2021) 238–250, https://doi.org/10.1016/j.semcancer.2020.04.002.

[8] A.S. Tagliafico, M. Piana, D. Schenone, R. Lai, A.M. Massone, N. Houssami, Overview of radiomics in breast cancer diagnosis and prognostication, Breast 49 (2020) 74–80, https://doi.org/10.1016/j.breast.2019.10.018.

[9] Y. Li, Y. Fan, D. Xu, Y. Li, Z. Zhong, H. Pan, B. Huang, X. Xie, Y. Yang, B. Liu, Deep learning radiomic analysis of DCE-MRI combined with clinical characteristics predicts pathological complete response to neoadjuvant chemotherapy in breast cancer, Front. Oncol. 12 (2022) 1041142, https://doi.org/10.3389/fonc.2022.1041142.

[10] Y. Yu, Z. He, J. Ouyang, Y. Tan, Y. Chen, Y. Gu, L. Mao, W. Ren, J. Wang, L. Lin, Z. Wu, J. Liu, Q. Ou, Q. Hu, A. Li, K. Chen, C. Li, N. Lu, X. Li, F. Su, Q. Liu, C. Xie, H. Yao, Magnetic resonance imaging radiomics predicts preoperative axillary lymph node metastasis to support surgical decisions and is associated with tumor microenvironment in invasive breast cancer: a machine learning, multicenter study, EBioMedicine 69 (2021) 103460, https://doi.org/10.1016/j.ebiom.2021.103460.

[11] X. Zheng, Z. Yao, Y. Huang, Y. Yu, Y. Wang, Y. Liu, R. Mao, F. Li, Y. Xiao, Y. Wang, Y. Hu, J. Yu, J. Zhou, Deep learning radiomics can predict axillary lymph node status in early-stage breast cancer, Nat. Commun. 11 (2020) 1236, https://doi.org/10.1038/s41467-020-15027-z.

[12] H.J. Lee, J.E. Lee, W.G. Jeong, S.Y. Ki, M.H. Park, J.S. Lee, Y.K. Nah, H.S. Lim, HER2-Positive breast cancer: association of MRI and clinicopathologic features with tumor-infiltrating lymphocytes, AJR Am. J. Roentgenol. 218 (2022) 258–269, https://doi.org/10.2214/AJR.21.26400.

[13] H.J. Aerts, E.R. Velazquez, R.T. Leijenaar, C. Parmar, P. Grossmann, S. Carvalho, J. Bussink, R. Monshouwer, B. Haibe-Kains, D. Rietveld, F. Hoebers, M. M. Rietbergen, C.R. Leemans, A. Dekker, J. Quackenbush, R.J. Gillies, P. Lambin, Decoding tumour phenotype by noninvasive imaging using a quantitative radiomics approach, Nat. Commun. 5 (2014) 4006, https://doi.org/10.1038/ncomms5006.

[14] J.J.M. van Griethuysen, A. Fedorov, C. Parmar, A. Hosny, N. Aucoin, V. Narayan, R.G.H. Beets-Tan, J.C. Fillion-Robin, S. Pieper, H. Aerts, Computational radiomics system to decode the radiographic phenotype, Cancer Res. 77 (2017) e104–e107, https://doi.org/10.1158/0008-5472.CAN-17-0339.

[15] E.J. Limkin, R. Sun, L. Dercle, E.I. Zacharaki, C. Robert, S. Reuze, A. Schernberg, N. Paragios, E. Deutsch, C. Ferte, Promises and challenges for the implementation of computational medical imaging (radiomics) in oncology, Ann. Oncol. 28 (2017) 1191–1206, https://doi.org/10.1093/annonc/mdx034.

[16] P. Lambin, R.T.H. Leijenaar, T.M. Deist, J. Peerlings, E.E.C. de Jong, J. van Timmeren, S. Sanduleanu, R. Larue, A.J.G. Even, A. Jochems, Y. van Wijk, H. Woodruff, J. van Soest, T. Lustberg, E. Roelofs, W. van Elmpt, A. Dekker, F.M. Mottaghy, J.E. Wildberger, S. Walsh, Radiomics: the bridge between medical imaging and personalized medicine, Nat. Rev. Clin. Oncol. 14 (2017) 749–762, https://doi.org/10.1038/nrclinonc.2017.141.

[17] B. Szekely, V. Bossuyt, X. Li, V.B. Wali, G.A. Patwardhan, C. Frederick, A. Silber, T. Park, M. Harigopal, V. Pelekanou, M. Zhang, Q. Yan, D.L. Rimm, G. Bianchini, C. Hatzis, L. Pusztai, Immunological differences between primary and metastatic breast cancer, Ann. Oncol. 29 (2018) 2232–2239, https://doi.org/10.1093/annonc/mdy399.

[18] L. Wu, S. Sun, F. Qu, M. Sun, X. Liu, Q. Sun, L. Cheng, Y. Zheng, G. Su, CXCL9 influences the tumor immune microenvironment by stimulating JAK/STAT pathway in triple-negative breast cancer, Cancer Immunol. Immunother. (2022), https://doi.org/10.1007/s00262-022-03343-w.

[19] Y.K. Liang, Z.K. Deng, M.T. Chen, S.Q. Qiu, Y.S. Xiao, Y.Z. Qi, Q. Xie, Z.H. Wang, S.C. Jia, D. Zeng, H.Y. Lin, CXCL9 is a potential biomarker of immune infiltration associated with favorable prognosis in ER-negative breast cancer, Front. Oncol. 11 (2021) 710286, https://doi.org/10.3389/fonc.2021.710286.

[20] Y. Li, M. Liang, Y. Lin, J. Lv, M. Chen, P. Zhou, F. Fu, C. Wang, Transcriptional expressions of CXCL9/10/12/13 as prognosis factors in breast cancer, J Oncol 2020 (2020) 4270957, https://doi.org/10.1155/2020/4270957.

[21] E. Razis, K.T. Kalogeras, I. Kotsantis, G.A. Koliou, K. Manousou, R. Wirtz, E. Veltrup, H. Patsea, N. Poulakaki, D. Dionysopoulos, S. Pervana, H. Gogas, A. Koutras, G. Pentheroudakis, C. Christodoulou, H. Linardou, K. Pavlakis, T. Koletsa, D. Pectasides, F. Zagouri, G. Fountzilas, The role of CXCL13 and CXCL9 in early breast cancer, Clin. Breast Cancer 20 (2020) e36–e53, https://doi.org/10.1016/j.clbc.2019.08.008.

[22] M. Pein, J. Insua-Rodriguez, T. Hongu, A. Riedel, J. Meier, L. Wiedmann, K. Decker, M.A.G. Essers, H.P. Sinn, S. Spaich, M. Sutterlin, A. Schneeweiss, A. Trumpp, T. Oskarsson, Metastasis-initiating cells induce and exploit a fibroblast niche to fuel malignant colonization of the lungs, Nat. Commun. 11 (2020) 1494, https://doi.org/10.1038/s41467-020-15188-x.

[23] S.R. Sompuram, K. Vani, A.K. Schaedle, A. Balasubramanian, S.A. Bogen, Quantitative assessment of immunohistochemistry laboratory performance by measuring analytic response curves and limits of detection, Arch. Pathol. Lab Med. 142 (2018) 851–862, https://doi.org/10.5858/arpa.2017-0330-OA.

[24] J. Vivian, A.A. Rao, F.A. Nothaft, C. Ketchum, J. Armstrong, A. Novak, J. Pfeil, J. Narkizian, A.D. Deran, A. Musselman-Brown, H. Schmidt, P. Amstutz, B. Craft, M. Goldman, K. Rosenbloom, M. Cline, B. O'Connor, M. Hanna, C. Birger, W.J. Kent, D.A. Patterson, A.D. Joseph, J. Zhu, S. Zaranek, G. Getz, D. Haussler, B. Paten, Toil enables reproducible, open source, big biomedical data analyses, Nat. Biotechnol. 35 (2017) 314–316, https://doi.org/10.1038/nbt.3772.

[25] Q. Yu, A. Wang, J. Gu, Q. Li, Y. Ning, J. Peng, F. Lv, X. Zhang, Multiphasic CT-based radiomics analysis for the differentiation of benign and malignant parotid tumors, Front. Oncol. 12 (2022) 913898, https://doi.org/10.3389/fonc.2022.913898.

[26] Y. Zheng, D. Zhou, H. Liu, M. Wen, CT-based radiomics analysis of different machine learning models for differentiating benign and malignant parotid tumors, Eur. Radiol. 32 (2022) 6953–6964, https://doi.org/10.1007/s00330-022-08830-3.

[27] Z. Li, L. Liu, Z. Zhang, X. Yang, X. Li, Y. Gao, K. Huang, A novel CT-based radiomics features analysis for identification and severity staging of COPD, Acad. Radiol. 29 (2022) 663–673, https://doi.org/10.1016/j.acra.2022.01.004.

[28] J. Wu, H. Zhang, L. Li, M. Hu, L. Chen, B. Xu, Q. Song, A nomogram for predicting overall survival in patients with low-grade endometrial stromal sarcoma: a population-based analysis, Cancer Commun. 40 (2020) 301–312, https://doi.org/10.1002/cac2.12067.

[29] Y. Liu, J. Wang, L. Li, H. Qin, Y. Wei, X. Zhang, X. Ren, W. Ding, X. Shen, G. Li, Z. Lu, D. Zhang, C. Qin, L. Tao, X. Chen, AC010973.2 promotes cell proliferation and is one of six stemness-related genes that predict overall survival of renal clear cell carcinoma, Sci. Rep. 12 (2022) 4272, https://doi.org/10.1038/s41598-022-07070-1.

[30] J. Xie, L. Chen, Q. Tang, W. Wei, Y. Cao, C. Wu, J. Hang, K. Zhang, J. Shi, M. Wang, A necroptosis-related prognostic model of uveal Melanoma was constructed by Single-cell sequencing analysis and weighted Co-expression network analysis based on public databases, Front. Immunol. 13 (2022) 847624, https://doi.org/10.3389/fimmu.2022.847624.

[31] Y. He, S. Duan, W. Wang, H. Yang, S. Pan, W. Cheng, L. Xia, X. Qi, Integrative radiomics clustering analysis to decipher breast cancer heterogeneity and prognostic indicators through multiparametric MRI, NPJ Breast Cancer 10 (2024) 72, https://doi.org/10.1038/s41523-024-00678-8.

[32] S. Zhu, S. Wang, S. Guo, R. Wu, J. Zhang, M. Kong, L. Pan, Y. Gu, S. Yu, Contrast-enhanced mammography radiomics analysis for preoperative prediction of breast cancer molecular subtypes, Acad. Radiol. 31 (2024) 2228–2238, https://doi.org/10.1016/j.acra.2023.12.005.

[33] P.O. Zinn, S.K. Singh, A. Kotrotsou, I. Hassan, G. Thomas, M.M. Luedi, A. Elakkad, N. Elshafeey, T. Idris, J. Mosley, J. Gumin, G.N. Fuller, J.F. de Groot, V. Baladandayuthapani, E.P. Sulman, A.J. Kumar, R. Sawaya, F.F. Lang, D. Piwnica-Worms, R.R. Colen, A coclinical radiogenomic validation study: conserved magnetic resonance radiomic appearance of periostin-expressing glioblastoma in patients and xenograft models, Clin. Cancer Res. 24 (2018) 6288–6299, https://doi.org/10.1158/1078-0432.CCR-17-3420.

[34] K.M. Panth, R.T. Leijenaar, S. Carvalho, N.G. Lieuwes, A. Yaromina, L. Dubois, P. Lambin, Is there a causal relationship between genetic changes and radiomics-based image features? An in vivo preclinical experiment with doxycycline inducible GADD34 tumor cells, Radiother. Oncol. 116 (2015) 462–466, https://doi.org/10.1016/j.radonc.2015.06.013.
[35] J. Schniering, M. Maciukiewicz, H.S. Gabrys, M. Brunner, C. Bluthgen, C. Meier, S. Braga-Lagache, A.C. Uldry, M. Heller, M. Guckenberger, H. Fretheim, C. T. Nakas, A.M. Hoffmann-Vold, O. Distler, T. Frauenfelder, S. Tanadini-Lang, B. Maurer, Computed tomography-based radiomics decodes prognostic and molecular differences in interstitial lung disease related to systemic sclerosis, Eur. Respir. J. 59 (2022), https://doi.org/10.1183/13993003.04503-2020.
[36] T. Vujasinovic, J. Pribic, K. Kanjer, N.T. Milosevic, Z. Tomasevic, Z. Milovanovic, D. Nikolic-Vukosavljevic, M. Radulovic, Gray-level Co-occurrence matrix texture analysis of breast tumor images in prognosis of distant metastasis risk, Microsc. Microanal. 21 (2015) 646–654, https://doi.org/10.1017/S1431927615000379.
[37] P.M. Marcovecchio, G. Thomas, S. Salek-Ardakani, CXCL9-expressing tumor-associated macrophages: new players in the fight against cancer, J Immunother Cancer 9 (2021), https://doi.org/10.1136/jitc-2020-002045.
[38] O. Lafci, P. Celepli, P. Seher Oztekin, P.N. Kosar, DCE-MRI radiomics analysis in differentiating luminal A and luminal B breast cancer molecular subtypes, Acad. Radiol. 30 (2023) 22–29, https://doi.org/10.1016/j.acra.2022.04.004.
[39] C. Militello, L. Rundo, M. Dimarco, A. Orlando, R. Woitek, I. D'Angelo, G. Russo, T.V. Bartolotta, 3D DCE-MRI radiomic analysis for malignant lesion prediction in breast cancer patients, Acad. Radiol. 29 (2022) 830–840, https://doi.org/10.1016/j.acra.2021.08.024.
[40] W.J. Tang, Q.C. Kong, Z.X. Cheng, Y.S. Liang, Z. Jin, L.X. Chen, W.K. Hu, Y.Y. Liang, X.H. Wei, Y. Guo, X.Q. Jiang, Performance of radiomics models for tumour-infiltrating lymphocyte (TIL) prediction in breast cancer: the role of the dynamic contrast-enhanced (DCE) MRI phase, Eur. Radiol. 32 (2022) 864–875, https://doi.org/10.1007/s00330-021-08173-5.
[41] A. Kadys, N. Gremke, L. Schnetter, K. Kostev, M. Kalder, Intercontinental comparison of women with breast cancer treated by oncologists in Europe, Asia, and Latin America: a retrospective study of 99,571 patients, J. Cancer Res. Clin. Oncol. 149 (2023) 7319–7326, https://doi.org/10.1007/s00432-023-04681-7.